Active Tuning of All-Dielectric Metasurfaces

Jürgen Sautter,[†] Isabelle Staude,[*,†] Manuel Decker,[†] Evgenia Rusak,[†] Dragomir N. Neshev,[†] Igal Brener,[‡] and Yuri S. Kivshar[†]

[†]Nonlinear Physics Centre and Centre for Ultrahigh Bandwidth Devices for Optical Systems (CUDOS), Research School of Physics and Engineering, The Australian National University, Canberra, ACT 2601, Australia and [‡]Center for Integrated Nanotechnologies, Sandia National Laboratories, Albuquerque, New Mexico 87185, United States

ABSTRACT All-dielectric metasurfaces provide a powerful platform for highly efficient flat optical devices, owing to their strong electric and magnetic dipolar response accompanied by negligible losses at near-infrared frequencies. Here we experimentally demonstrate dynamic tuning of electric and magnetic resonances in all-dielectric silicon nanodisk metasurfaces in the telecom spectral range based on the temperature-dependent refractive-index change of a nematic liquid crystal. We achieve a maximum resonance tuning range of 40 nm and a pronounced change in the transmittance intensity up to a factor of 5. Strongly different tuning rates are observed for the electric and the magnetic response, which allows for dynamically adjusting the spectral mode separation. Furthermore, we experimentally investigate the influence of the anisotropic (temperature-dependent) dielectric environment provided by the liquid crystal on both the electric and magnetic resonances. We demonstrate that the phase transition of the liquid crystal from its nematic to its isotropic phase can be used to break the symmetry of the optical metasurface response. As such, our approach allows for spectral tuning of electric and magnetic resonances of all-dielectric metasurfaces as well as switching of the anisotropy of the optical response of the device.

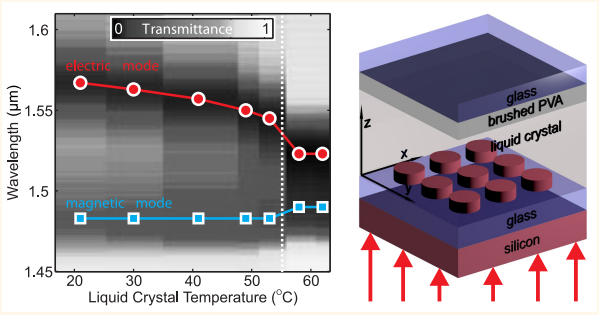

KEYWORDS: high-permittivity nanoparticles · metasurfaces · liquid crystals · tunable metamaterials · nanostructures · optical anisotropy

Designer metasurfaces[1]—planar arrangements of designed, nanostructured building blocks (meta-atoms)—have recently attracted a lot of attention due to their potential to provide flat, ultrathin components for a multitude of optical functionalities, including polarization manipulation, sensing, dispersion engineering, and emission control, to name just a few.[2] Most prominently, their ability to create arbitrary wavefronts by engineering the spatial distribution of phase discontinuities has recently stimulated revolutionary developments in the field of wavefront engineering.[3−7] All these functionalities are typically achieved by simple transmission of light through (or reflection from) a metasurface, a single-layer metamaterial composed of nanoscale resonators. To date, the vast majority of optical metasurfaces have been based on *metallic resonators* supporting localized surface plasmon resonances.[1−7] However, the efficiency of such plasmonic metasurfaces is strongly limited by the inherent losses of metals at optical frequencies.

Thus, *all-dielectric* metasurfaces consisting of planar arrangements of high-refractive-index dielectric nanoparticles with tailored optical properties have emerged as a new paradigm for controlling and manipulating lightwaves at the nanoscale. Owing to their low losses in the visible and near-infrared spectral range, all-dielectric metasurfaces allow for the realization of practically absorptionless functional devices for wavefront manipulation.[8−11] Similar to the plasmonic resonances of metallic nanoparticles, all-dielectric nanoparticles exhibit strong localized resonances in the optical spectral range, which can be tailored *via* their size, shape, and material composition. Importantly, for nanoparticles composed of high-refractive-index dielectric materials, *e.g.*, silicon, these resonances can be of both electric and magnetic multipolar character,[12−15] the

* Address correspondence to isabelle.staude@anu.edu.au.

Received for review February 1, 2015 and accepted March 8, 2015.

Published online March 09, 2015
10.1021/acsnano.5b00723

latter originating from the optical excitation of circular displacement currents inside the dielectric nanoparticles. The combination of low losses and both electric and magnetic dipolar resonances with resonance properties that can be tailored at will is key to engineered metasurfaces for wavefront and dispersion engineering with near-unity efficiency in transmission.[11] Furthermore, the low dissipative losses of all-dielectric metasurfaces allow for the formation of optical resonances with higher quality factors as compared to their plasmonic counterparts. This is particularly interesting for dielectric metasurface modes exhibiting additionally low radiative losses, sometimes called dark modes, which can be coupled to the far-field indirectly through optical Fano resonances.[16−18] Such modes can exhibit very sharp spectral features, making them promising candidates for sensors[17,18] and narrow spectral filters.[16]

However, as optical metasurfaces become relevant for practical applications, the capability of actively controlling their optical properties becomes increasingly important. The ability to dynamically and reversibly shift the spectral position of the metasurface resonances as a function of an externally controllable parameter is essential for the realization of, for example, tunable spectral filters, active emission control, and dynamically adjustable flat optical components such as lenses, beam shapers, and holograms. For plasmonic metasurfaces and metamaterials a number of tuning and switching mechanisms have been realized so far.[19] A first class of approaches is based on the mechanical reconfiguration of the metamaterial structure, which can be induced by various external parameters, e.g., temperature and voltage. For example, optical metamaterials fabricated on bimaterial bridges[20] have been successfully demonstrated to allow for significant and controllable tuning of the metamaterial resonances. A second class of approaches utilizes the interaction of the metamaterials with phase-change materials such as vanadium dioxide[21] or chalcogenide glasses.[22] Other tuning schemes, which have been successfully demonstrated for THz and infrared metamaterials, include free-carrier injection in semiconductors,[23] voltage-controlled strong coupling of a metamaterial resonance to an intersubband transition,[24] and metamaterials exploiting the modification of the electromagnetic response of graphene using an applied voltage.[25,26]

Finally, considerable efforts have been concentrated on tuning and switching of plasmonic metamaterials using liquid crystals (LCs).[27−35] Liquid crystals are a well-established and affordable technology and can offer a highly practical solution for the dynamic control of metamaterial optical properties as long as they are compatible with the requirements for the operation temperature and switching times.[19] LC tunable metamaterials can be implemented in various ways, making use of either the strong temperature dependence of the LC optical anisotropy, the realignment of the LCs by an external electric or magnetic field, or the LC's strong nonlinear response. Initially, LC tuning of the electromagnetic properties of metamaterials through various mechanisms were mainly explored at GHz or THz frequencies,[19,30,33] where the near-fields of the metamaterial modes extend over several micrometers up to millimeters, thus rendering them less sensitive to surface effects such as the alignment of the LC molecules in the immediate vicinity of the relevant material interfaces. At optical frequencies, thermal,[27] all-optical,[29,31] and electro-optic[32,34,35] LC tuning or switching of metamaterial resonances have also been demonstrated. A big challenge for optical LC tunable plasmonic metasurfaces is that the thickness of the LC layer, which is affected by anchoring of the LC molecules to the surface, is comparable to the extension of the optical near-fields of the metasurface. In plasmonic metasurfaces, the LC anchoring has therefore been found to largely suppress the conventional tuning and switching mechanisms in plasmonic metasurfaces unless the anchoring is reduced by surface functionalization[35] or the anchoring itself is incorporated into the metasurface design as a functionality-providing feature.[32,34]

Thus, dynamic control of metamaterials and metasurfaces has seen tremendous progress in the recent past, but was exclusively focused on *plasmonic* structures. Active tuning in the emerging field of *all-dielectric* metasurfaces, however, has neither been attempted nor demonstrated so far. Closing this gap would allow for the realization of dynamically controlled highly efficient flat optical devices such as reconfigurable metasurface beam shapers and holograms.

Here we realize dynamic tuning of electric and magnetic resonances in all-dielectric silicon nanodisk metasurfaces at near-infrared frequencies based on the temperature-dependent refractive-index change of a nematic liquid crystal. We also experimentally investigate the influence of the anisotropic (temperature-dependent) dielectric environment provided by the LC on the electric and magnetic resonances. Furthermore, we demonstrate switching of the optical isotropy of the metasurface by employing a phase transition of the LC from nematic to isotropic and *vice versa*. Our results establish an all-dielectric metasurface integrated into LC cells as an important method to realize tunable and switchable all-dielectric metadevices for wavefront manipulation.

RESULTS AND DISCUSSION

Description of the Experimental System. In our work we use an all-dielectric metasurface composed of silicon nanodisks integrated into an LC cell as shown in Figure 1a. The individual nanodisk height is h = 220 nm and their diameter is d = 606 nm. The nanodisks are arranged in a subwavelength periodic square-array

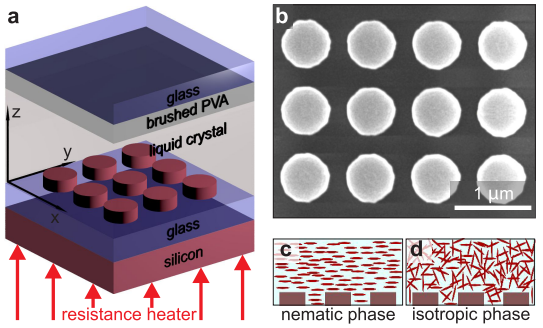

Figure 1. (a) Schematic of the silicon nanodisk metasurface integrated into an LC cell. The silicon nanodisk sample is immersed in the LC, and the cell is covered by a layer of brushed PVA for alignment of the LC. The cell can be heated by a resistor mounted on the backside of the silicon handle wafer. (b) Scanning electron micrograph of the silicon nanodisk metasurface. (c, d) Sketch of the (idealized) arrangement of the LC molecules in the nematic and the isotropic phase, respectively.

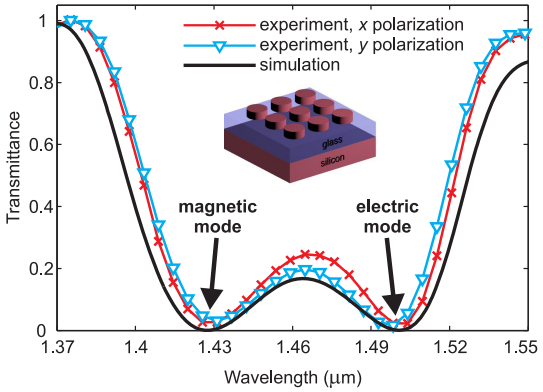

Figure 2. Measured and calculated transmittance spectra of the sample before infiltration of the cell with the LC.

with a lattice constant a = 919 nm. Figure 1b shows a scanning electron microscope (SEM) image of the nanodisk metasurface. The height of the LC cell is 170 μm, covered by a glass substrate that is coated with a functional layer of poly(vinyl alcohol) (PVA), inducing preferred alignment of the liquid crystal in the x-direction. Details of the sample fabrication and assembly of the LC cell can be found in the Methods section. We use the Licristal E7 LC from Merck, which features a strong optical anisotropy along the axis of the LC molecules in its nematic phase. At room temperature the refractive indices at λ = 1.55 μm are n_o = 1.51 and n_e = 1.70. At $T \approx$ 58 °C the LC undergoes a phase transition, switching from its nematic to its isotropic phase with a refractive index of n_{iso} = 1.55.[36] The infiltration of the LC was performed in the isotropic phase at $T \approx$ 90 °C. Figure 1c,d illustrate the (idealized) arrangement of the LC molecules in the respective phases. In our experiments, the temperature of the LC is controlled by resistance heating of the silicon handle wafer.

For the measurements of the linear transmittance spectra of the silicon nanodisk metasurface we illuminated the sample with a halogen lamp and measured the transmittance spectrum with an optical spectrum analyzer. A pair of 20× Mitutoyo Plan Apo NIR infinity-corrected objectives with numerical aperture NA = 0.4 is used for focusing the incident light onto the sample and collecting the light transmitted through it. A wire-grid polarizer was used to define the polarization of the incident light. The sample was illuminated from the backside such that, after the subsequent LC infiltration, the incident light was first transmitted through the nanodisk metasurface before passing through the LC. In this fashion the polarization direction at which the silicon nanodisk structure is excited is independent of the orientation of the LC molecules in the bulk of the LC volume. The spectra are referenced to the transmittance of the cell next to the metasurface, taking into account the layered wafer structure of the sample.

We first measure the transmittance spectra of the nanodisk metasurface without the LC along the two symmetry axes of the square array as a reference. We confirm that the system shows a highly isotropic response under a polarization rotation of 90 deg of the incident light due to the symmetry of the structure (see Figure 2). We compare these results with numerical calculations using CST Microwave Studio (see Methods for details), showing excellent agreement with the experimental spectra. The resonance at $\lambda \approx$ 1.43 μm corresponds to the magnetic dipole mode, whereas the resonance at $\lambda \approx$ 1.50 μm is the electric dipole mode of the silicon nanodisks.[11,14]

Numerical Model. Next, to investigate the effect of LC infiltration on the optical properties of the metasurface, we numerically calculate the transmittance spectra of the silicon nanodisk metasurface covered by an ideal LC for x- and y-polarized incident light. These results are shown in Figure 3a. The numerical spectra of the metasurface without LC are also included for comparison (black line in Figure 3a). Details of the numerical calculations are provided in the Methods section. First we consider infiltration with the LC in its isotropic phase (green line in Figure 3a). For this case, the LC is modeled as a homogeneous medium with a refractive index of n = 1.55.[36] After LC infiltration, both resonances are red-shifted as a consequence of the higher effective refractive index of the LC in comparison to the refractive index of air. Due to symmetry and the isotropic environment, the spectra remain degenerate for x- and y-polarized incident light. Second, we consider infiltration with the LC in its nematic phase (red and cyan lines in Figure 3a for x- and y-polarization, respectively). For this case we model the LC as an anisotropic medium with its anisotropy axis oriented in the x-direction, n_o = 1.51 and n_e = 1.70.[36] As such, for x-polarized light the electric field is parallel to n_e; for y-polarization the electric field is aligned parallel to n_o.

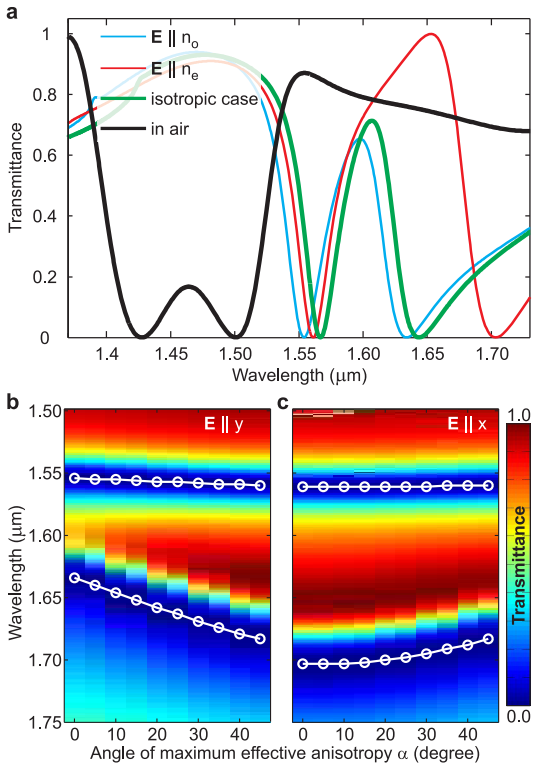

Figure 3. Numerical results: (a) Transmittance spectra of the silicon nanodisk metasurface for *x*- and *y*-polarized incident light before (black line) and after infiltration with LC in its isotropic (green line) and nematic (red and cyan lines) phase. In the latter case, the anisotropy axis of the LC is oriented along the *x*-direction. (b, c) Transmittance spectra for a systematic variation of the in-plane orientation of the anisotropy axis for (b) *y*- and (c) *x*-polarization.

In addition to a red-shift as compared to the uninfiltrated case, we observe a symmetry break in the optical response along the two axes of the lattice (*x*- and *y*-direction) due to the optical anisotropy introduced by the aligned LC at room temperature. This LC anisotropy breaks the polarization degeneracy for both the electric and the magnetic mode, resulting in different resonance positions depending on the polarization of the incident light (red and cyan lines in Figure 3a). This polarization splitting is much more pronounced for the electric resonance, where it is 69 nm. For the magnetic resonance it is 7 nm.

Refinement of the Numerical Model. So far we have considered only the ideal case of perfect unidirectional alignment of the LC molecules in the *x*-direction. However, in the vicinity of the nanostructured surface one can expect the LC alignment to be influenced by the topography and surface properties of the sample. As a consequence, the simple model assuming effective bulk properties for the LC needs to be refined. However, a comprehensive description of the LC behavior—a multilevel feedback system—on a molecular level, is highly complex[37] and impractical for large simulation volumes as present in our system. Thus, in order to investigate the influence of the LC alignment on the optical transmittance spectra in a simple fashion, we continue describing our system by a macroscopic (bulk) approach, utilizing that it is dependent on the effective refractive index in the vicinity of the nanodisks only. However, we now refine our model to include a perturbation, extending our effective index calculations to such cases where the anisotropy axis no longer coincides with the *x*-axis but still lies in the *x*−*y*-plane. This way, we keep the assumption that a planar alignment of the LC molecules is favored by the presence of the top alignment layer at the opposite side of the LC cell. Within the *x*−*y*-plane, we then rotate the anisotropy axis from 0 to 45 deg with respect to the *x*-axis in 5 deg steps and investigate the effect on the transmittance spectra. The results of these calculations are shown in Figure 3b,c for *y*- and *x*-polarization of the incident light, respectively. The angle between the anisotropy axis and the *x*-axis is denoted by α. As we increase α, we effectively emulate a reduction of anisotropy for *x*- and *y*-polarized incident light, with $n_{x,\mathrm{eff}} = n_o + (n_e - n_o)\cos(\alpha)$ and $n_{y,\mathrm{eff}} = n_o + (n_e - n_o)\sin(\alpha)$. This results in a reduction of the difference between the spectral mode positions for *x*- and *y*-polarization, finally leading to identical transmittance spectra for the two orthogonal polarizations of the incident light at α = 45°. These results for oblique alignment angles probed along the lattice directions provide us with a prediction for the transmittance spectra of the system in the case of planar, but non-ideal alignment of the LC molecules in the region corresponding to the optical near-fields of the silicon nanodisk structure. In the following these results can be used to extract an effective orientation of the anisotropy axis in experiments.

Experimental Results. First, we experimentally infiltrate the cell incorporating the sample from Figure 2 with an LC. We then measure the sample's transmittance at room temperature, where the LC is in its nematic phase. The measured spectra are shown in Figure 4a. They have been normalized to the transmittance through the LC cell, including the layered structure of the silicon-on-insulator wafer. For *y*-polarization (cyan line) the electric resonance shifts to $\lambda = 1.65\,\mu$m, while for *x*-polarization (red line) it shifts to $\lambda = 1.68\,\mu$m. The magnetic resonance shifts to $\lambda \approx 1.55\,\mu$m with only a slight splitting observed for *x*-polarization (red line) and *y*-polarization (cyan line). The observed Fabry–Perot oscillations stem from the finite thickness of the LC cell.

Next, we apply a dc current to the resistor mounted on the backside of the handle wafer to heat the LC cell to $T = 62\,^{\circ}$C, thereby switching the phase of the LC from nematic to isotropic. In the isotropic phase, the experimental transmittance spectra for *x*- and *y*-polarized incident light (red and cyan dashed lines in Figure 4a) are nearly identical again. This means that the optical anisotropy of the nanodisk metasurface is fully

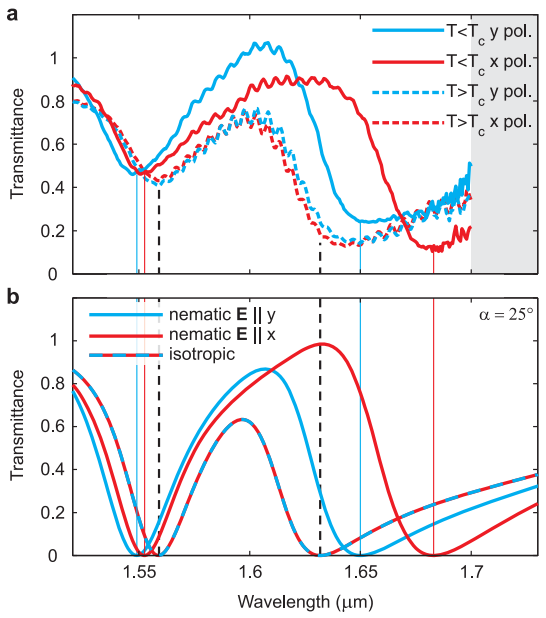

Figure 4. (a) Measured normalized transmittance spectra for the same sample shown in Figure 2 after LC infiltration. Room-temperature spectra are displayed in red and cyan for *x*- and *y*-polarized incident light, respectively. Heating the sample above the LC phase transition temperature ($T \geq$ 58 °C) induces a pronounced blue-shift for the electric resonance and a slight red-shift for the magnetic resonance, resulting in identical spectra for *x*- and *y*-polarization (red and cyan dashed lines) as the LC switches from its nematic to its isotropic phase. (b) Corresponding numerically calculated transmittance spectra, using experimental values from ref 36 for the refractive indices of the LC, $\alpha = 25°$, and taking imperfections regarding the LC infiltration into account. The vertical lines mark the spectral positions of the resonance minima in the calculated spectra in order to facilitate quantitative comparison with the experimentally obtained values.

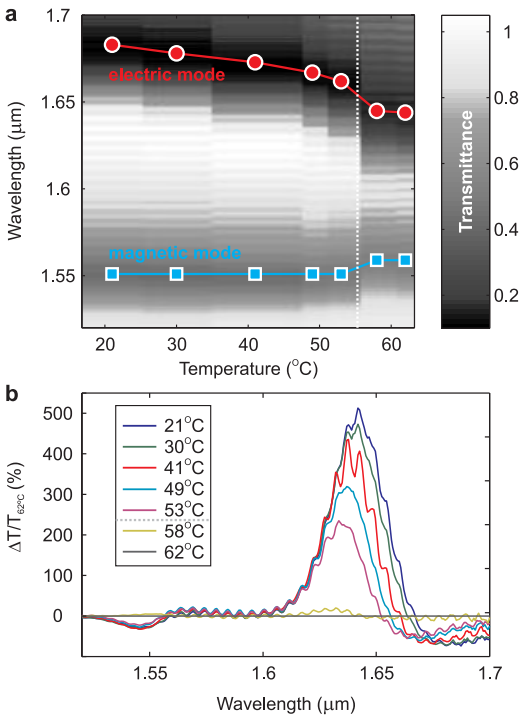

Figure 5. (a) Experimentally measured transmittance spectra of the metasurface from Figure 4 (h = 220 nm, d = 606 nm, and a = 919 nm) for *x*-polarized light and a systematic variation of the temperature. The resonance positions of the electric resonance are plotted as red dots; the resonance positions of the magnetic resonance, as cyan squares. The phase transition is indicated by the white dashed line. (b) Transmittance contrast ($\Delta T/T_{62\ °C} = (T_i - T_{62\ °C})/T_{62\ °C}$) of the nanodisk metasurface spectrum at the temperatures i relative to the isotropic metasurface response (for a temperature of 62 °C).

removed and the high symmetry of the sample's optical response is restored. For the isotropic case, the electric resonances appear at $\lambda = 1.64\ \mu$m for both polarizations, while the magnetic resonance is at $\lambda =$ 1.56 μm. The switching time is on the order of seconds in both directions.

By applying our previous theoretical model to the experimental system (see Methods section for details) and comparing the results with the experimentally measured resonance positions for *x*- and *y*-polarized incident light, we estimate that the effective anisotropy realized in our structure corresponds to an average in-plane orientation of the LC molecules of ±25 deg. The calculated spectra are displayed in Figure 4b and show excellent agreement with the experimental data in Figure 4a. All the essential features, namely, the resonance shifts and the switching of the anisotropy of the sample, are well reproduced, and good quantitative agreement is obtained for all resonance positions. The deviations regarding the resonance depths found in the experimental and calculated spectra are likely due to alignment inhomogeneities in the bulk of the LC in the experiment, leading to increased scattering.

Finally, to investigate the tuning capability of our all-dielectric metasurface, we record the sample's transmittance for *x*-polarization when we subsequently increase the LC temperature from T = 21 °C (nematic/anisotropic phase) to above the phase transition temperature ($T \geq$ 58 °C, isotropic phase) and demonstrate dynamic resonance tuning due to the temperature-dependent refractive-index change of the LC. Figure 5a shows the temperature-dependent spectra and spectral shift of the electric and magnetic resonance for *x*-polarized incident light. We observe a significant spectral shift of the electric resonance for increasing temperatures, while the magnetic resonance remains at approximately the same spectral position below the phase transition temperature. Importantly, we can clearly observe the phase transition from the nematic to the isotropic phase of the LC at $T \approx$ 58 °C, resulting in a pronounced spectral shift (last two data points in Figure 5a) for both the electric and the magnetic resonance. Note also that the resonances are shifted in opposite directions. The maximum tuning range realized in our experiment amounts to approximately 40 nm and is observed for the electric dipole resonance. In order to quantify the strength of the transmittance change associated with the

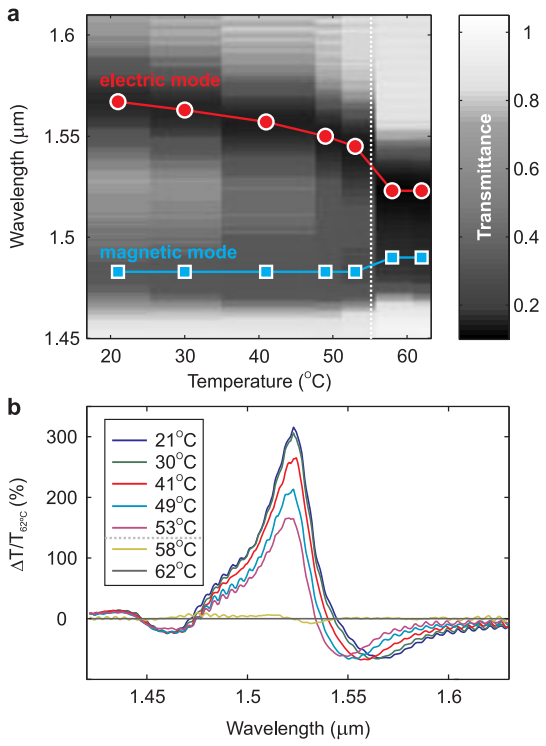

Figure 6. Experimental results: (a) Temperature-dependent *x*-polarized transmittance spectra for a sample with reduced disk radius and lattice constant (h = 220 nm, d = 560 nm, a = 860 nm). The resonance positions of the electric/magnetic resonances are plotted as red dots/cyan squares, respectively. The phase transition is indicated by the white dashed line. (b) Transmittance contrast ($\Delta T/T_{62\ °C} = (T_i - T_{62\ °C})/T_{62\ °C}$) of the nanodisk metasurface spectrum at the temperatures i relative to the isotropic metasurface response (for a temperature of 62 °C).

resonance tuning of our LC-infiltrated all-dielectric metasurface, in Figure 5b we also plot the spectrally resolved transmittance contrast, defined as the relative change of the transmittance $\Delta T_i/T_{62\ °C} = (T_i - T_{62\ °C})/T_{62\ °C}$ for the temperatures i with respect to the transmittance spectrum at T = 62 °C (isotropic phase).[20] We observe a maximum transmittance contrast of $\Delta T_{21\ °C}/T_{62\ °C} \approx 30\%$ for the magnetic mode and of $\Delta T_{21\ °C}/T_{62\ °C} \approx 500\%$ for the electric mode. This maximum transmittance contrast occurs at λ = 1.642 μm and is associated with a transmittance change of 0.84 from near-unity transmittance at T = 21 °C to a transmittance value of about 0.16 at 62 °C.

Importantly, the differences in the tuning rates observed for the electric and magnetic modes allow us to dynamically tune the relative positions of the resonances with respect to each other. In order to demonstrate how this behavior can be used to introduce not only shifts in the spectral resonances positions but strong qualitative changes in the spectral shape of the transmittance spectra of a silicon metasurface, we repeat the measurement for a sample exhibiting both a reduced disk radius and reduced lattice constant (h = 220 nm, d = 560 nm, a = 860 nm). The spectral separation between the electric and the magnetic dipole mode in an isotropic environment is known to be dependent on the height-to-diameter aspect ratio of the nanodisks.[14] Thus, by choosing the dimensions of the second sample such that the nanodisk aspect ratio is increased with respect to the previous sample, we induce a decrease of the spectral mode separation. We then repeat the temperature tuning experiment for the second sample and obtain the results shown in Figure 6a. While a similar tuning behavior to that for the first sample is observed below the phase transition temperature, as the system undergoes a phase transition to the isotropic phase, the spectral separation between the electric and the magnetic mode is reduced to such an extent that the transmittance spectrum changes from a two-dip shape to an effective single-dip shape as the separation between the resonances becomes comparable to their width. Note that the spectral position of the global minimum around 1.525 μm in the isotropic phase coincides well with that of the (nonresonant) local maximum in between the two separate resonances in the nematic phase at room temperature. The transmittance contrast for the second sample is shown in Figure 6b and also features a strong signal modulation at telecommunication frequencies around 1.5 μm. The maximum transmittance contrast appears at λ = 1.523 μm with a transmittance change of 0.45 from a transmittance value of 0.59 at T = 21 °C to 0.14 at 62 °C.

CONCLUSIONS

We have experimentally realized active tuning of all-dielectric metasurfaces exhibiting both electric and magnetic optically induced resonances, with a maximum tuning range of 40 nm for the electric resonance and with a transmission contrast of up to 500% at near-infrared frequencies. We have also demonstrated that the strong optical anisotropy of the LC in combination with its phase transition to the isotropic phase can be utilized to dynamically switch the symmetry of the optical response of the metasurface and, hence, to dynamically induce a symmetry break in the isotropy of the metasurface response. Our system is based on a highly symmetric silicon nanodisk metasurface integrated into an LC cell that is heated from room temperature to temperatures above the phase transition point of the LC in order to investigate both resonance tuning due to the temperature dependence of the LC refractive index and the symmetry switching of the optical response. Our experimental results are in excellent agreement with numerical simulations that model the macroscopic LC response by a uniaxial anisotropic refractive index tensor and treat the nanostructure-induced perturbations of the LC-molecule alignment as effective reorientation of the LC anisotropy axis. The large tuning range and transmittance contrast observed for the silicon nanodisk metasurface in the

near-infrared spectral range shows that surface anchoring of the LC molecules does not play a dominant role in this system. Our work opens up a route toward dynamically tunable and switchable all-dielectric metasurface devices. In order to further improve on the control and speed of the switching process, reorientation of the LC anisotropy axis within the nematic phase by application of an external electric or magnetic field can be considered, providing faster switching times for the transition from the "off" to the "on" state.[32] Moreover, the ability to dynamically shift the electric and magnetic dipole resonance positions with respect to each other is of particular interest for actively tunable silicon Huygens' metasurfaces,[11] which can enable near-unity transmission-efficiency wavefront manipulation devices.

METHODS

Sample Fabrication and Assembly of the LC Cell. The silicon nanodisk samples are fabricated *via* electron-beam lithography on silicon-on-insulator wafers (SOITEC, 220 nm top silicon thickness, 2 μm buried oxide thickness, backside polished) using the negative-tone electron-beam resist NEB-31A. The resulting resist pattern is used as a mask for reactive-ion etching. The residual resist is removed by oxygen plasma etching. For assembly of the LC cell, 170 μm thick glass spacers are placed around the nanodisk arrays to define the height of the LC cell. The thickness is chosen to minimize the influence of Fabry–Perot oscillations within the optical cavity formed by the LC cell on the optical spectra of the metasurface. For the chosen spacer thickness these oscillations occur at a period much smaller than the spectral width of the relevant Mie-type resonances of the silicon nanodisk meta-atoms. The LC cell is covered with a glass substrate onto which we spin-coated a layer of 6.3% hydrolyzed poly(vinyl alcohol) (PVA, 3000 rpm, 90 s). The PVA layer is mechanically brushed to create a preferred linear alignment direction for the LC. For infiltration of the fully assembled cell with the LC, both the LC and the cell are heated to $T = 90$ °C to enable infiltration in the isotropic phase. Finally, a resistor (WELWYN WH10 15R JI) is mounted on the backside of the wafer. Application of a dc current to the resistor allows us to heat the sample and to control the temperature of the cell in the experiment.

Numerical Calculations. All numerical calculations are performed using the commercial software package CST Microwave Studio. In order to reproduce the experimental situation as accurate as possible, we explicitly take into account the influence of the handle wafer. We also mimick the experimental referencing procedure to the LC cell without the silicon nanodisk structure for comparison with experimental data. For temperatures below the phase transition point the LC is modeled as a 2 μm thick layer of an anisotropic uniaxial medium with $n_{xx} = n_e = 1.70$ and $n_{yy} = n_o = 1.51$, respectively.[36] For temperatures above the phase transition point the LC is represented as an isotropic medium with a refractive index of $n = 1.55$.[36] The refractive index of the silicon is taken to be 3.5; that of the silicon oxide is 1.45. All materials are assumed to be lossless and dispersionless. We use unit-cell boundaries in the *x*- and *y*-direction and open boundaries in the *z*-direction. For direct comparison with experimental data, the effect of incomplete infiltration of the silicon nanodisk structure has been taken into account by including a shallow air layer between the silica substrate and the LC layer, with a thickness of 20 nm determined by the size of the shift after initial infiltration of the sample with the LC.

Conflict of Interest: The authors declare no competing financial interest.

Acknowledgment. The authors acknowledge the support from the Australian Research Council through Centre of Excellence, Discovery Project, and DECRA Fellowship grants. This work was performed, in part, at the Center for Integrated Nanotechnologies, an Office of Science User Facility operated for the U.S. Department of Energy (DOE) Office of Science. Sandia National Laboratories is a multiprogram laboratory managed and operated by Sandia Corporation, a wholly owned subsidiary of Lockheed Martin Corporation, for the U.S. Department of Energy's National Nuclear Security Administration under contract DE-AC04-94AL85000. E.R. acknowledges the support from the German National Academic Foundation.

REFERENCES AND NOTES

1. Yu, N.; Capasso, F. Flat Optics with Designer Metasurfaces. *Nat. Mater.* **2014**, *13*, 139–150.
2. Kildishev, A. V.; Boltasseva, A.; Shalaev, V. M. Planar Photonics with Metasurfaces. *Science* **2013**, *339*, 1232009.
3. Yu, N.; Genevet, P.; Kats, M. A.; Aieta, F.; Tetienne, J.-P.; Capasso, F.; Gaburro, Z. Light Propagation with Phase Discontinuities: Generalized Laws of Reflection and Refraction. *Science* **2011**, *334*, 333–337.
4. Ni, X.; Emani, N. K.; Kildishev, A. V.; Boltasseva, A.; Shalaev, V. M. Broadband Light Bending with Plasmonic Nanoantennas. *Science* **2012**, *335*, 427.
5. Chen, X.; Huang, L.; Mühlenbernd, H.; Li, G.; Bai, B.; Tan, Q.; Jin, G.; Qiu, C.-W.; Zhang, S.; Zentgraf, T. Dual-Polarity Plasmonic Metalens for Visible Light. *Nat. Commun.* **2012**, *3*, 1198.
6. Larouche, S.; Tsai, Y.-J.; Tyler, T.; Jokerst, N. M.; Smith, D. R. Infrared Metamaterial Phase Holograms. *Nat. Mater.* **2012**, *11*, 450–454.
7. Huang, L.; Chen, X.; Mühlenbernd, H.; Zhang, H.; Chen, S.; Bai, B.; Tan, Q.; Jin, G.; Cheah, K.-W.; Qiu, C.-W.; *et al.* Three-Dimensional Optical Holography Using a Plasmonic Metasurface. *Nat. Commun.* **2013**, *4*, 2808.
8. Zou, L.; Withayachumnankul, W.; Shah, C. M.; Mitchell, A.; Bhaskaran, M.; Sriram, S.; Fumeaux, C. Dielectric Resonator Nanoantennas at Visible Frequencies. *Opt. Express* **2013**, *21*, 1344–1352.
9. Yang, Y.; Wang, W.; Moitra, P.; Kravchenko, I. I.; Briggs, D. P.; Valentine, J. Dielectric Meta-Reflect Array for Broadband Linear Polarization Conversion and Optical Vortex Generation. *Nano Lett.* **2014**, *14*, 1394–1399.
10. Lin, D.; Fan, P.; Hasman, E.; Brongersma, M. L. Dielectric Gradient Metasurface Optical Elements. *Science* **2014**, *345*, 298.
11. Decker, M.; Staude, I.; Falkner, M.; Dominguez, J.; Neshev, D. N.; Brener, I.; Pertsch, T.; Kivshar, Yu. S. High-Efficiency Dielectric Huygens Surfaces, *Adv. Opt. Mater.* **2015**, Early View, DOI: 10.1002/adom.201400584.
12. Evlyukhin, A. B.; Novikov, S. M.; Zywietz, U.; Eriksen, R. L.; Reinhardt, C.; Bozhevolnyi, S. I.; Chichkov, B. N. Demonstration of Magnetic Dipole Resonances of Dielectric Nanospheres in the Visible Region. *Nano Lett.* **2012**, *12*, 3749–3755.
13. Kuznetsov, A. I.; Miroshnichenko, A. E.; Fu, Y. H.; Zhang, J.; Luk'yanchuk, B. Magnetic Light. *Sci. Rep.* **2012**, *2*, 492.
14. Staude, I.; Miroshnichenko, A. E.; Decker, M.; Fofang, N. T.; Liu, S.; Gonzales, E.; Dominguez, J.; Luk, T. S.; Neshev, D. N.; Brener, I.; *et al.* Tailoring Directional Scattering through Magnetic and Electric Resonances in Subwavelength Silicon Nanodisks. *ACS Nano* **2013**, *7*, 7824–7832.
15. Staude, I.; Khardikov, V. V.; Fofang, N. T.; Liu, S.; Decker, M.; Neshev, D. N.; Luk, T. S.; Brener, I.; Kivshar, Yu. S. Shaping Photoluminescence Spectra with MagnetoelectricResonances in All-Dielectric Nanoparticles. *ACS Photonics* **2015**, *2*, 172–177.
16. Wu, C.; Arju, N.; Kelp, G.; Fan, J. A.; Dominguez, J.; Gonzales, E.; Tutuc, E.; Brener, I.; Shvets, G. Spectrally Selective Chiral

Silicon Metasurfaces Based on Infrared Fano Resonances. *Nat. Commun.* **2014**, *5*, 3892.
17. Chong, K. E.; Hopkins, B.; Staude, I.; Miroshnichenko, A. E.; Dominguez, J.; Decker, M.; Neshev, D. N.; Brener, I.; Kivshar, Yu. S. Observation of Fano Resonances in All-Dielectric Nanoparticle Oligomers. *Small* **2014**, *10*, 1985–1990.
18. Yang, Y.; Kravchenko, I. I.; Briggs, D. P.; Valentine, J. All-Dielectric Metasurface Analogue of Electromagnetically Induced Transparency. *Nat. Commun.* **2014**, *5*, 5753.
19. Zheludev, N. I.; Kivshar, Yu. S. From Metamaterials to Metadevices. *Nat. Mater.* **2012**, *11*, 917–924.
20. Ou, J. Y.; Plum, E.; Jiang, L.; Zheludev, N. I. Reconfigurable Photonic Metamaterials. *Nano Lett.* **2011**, *11*, 2142–2144.
21. Driscoll, T.; Kim, H.-T.; Chae, B.-G.; Kim, B.-J.; Lee, Y.-W.; Jokerst, N. M.; Palit, S.; Smith, D. R.; di Ventra, M.; Basov, D. N. Memory Metamaterials. *Science* **2009**, *325*, 1518–1521.
22. Samson, Z. L.; MacDonald, K. F.; de Angelis, F.; Gholipour, B.; Knight, K.; Huang, C. C.; Die Fabrizio, E.; Hewak, D. W.; Zheludev, N. I. Metamaterial Electro-Optic Switch of Nanoscale Thickness. *Appl. Phys. Lett.* **2010**, *96*, 141305.
23. Chen, H.-T.; O'Hara, J. F.; Azad, A. K.; Taylor, A. J.; Averitt, R. D.; Shrekenhamer, D. B.; Padilla, W. J. Experimental Demonstration of Frequency-Agile Terahertz Metamaterials. *Nat. Photonics* **2008**, *2*, 295–298.
24. Benz, A.; Montaño, I.; Klem, J. F.; Brener, I. Tunable Metamaterials Based on Voltage Controlled Strong Coupling. *Appl. Phys. Lett.* **2013**, *103*, 263116.
25. Ju, L.; Geng, B.; Horng, J.; Girit, C.; Martin, M.; Hao, Z.; Bechtel, H. A.; Liang, X.; Zettl, A.; Shen, Y. R.; *et al*. Graphene Plasmonics for Tunable Terahertz Metamaterials. *Nat. Nanotechnol.* **2011**, *6*, 630–634.
26. Mousavi, S. H.; Kholmanov, I.; Alici, K. B.; Purtseladze, D.; Arju, N.; Tatar, K.; Fozdar, D. Y.; Suk, J. W.; Hao, Y.; Khanikaev, A. B.; *et al*. Inductive Tuning of Fano-Resonant Metasurfaces Using Plasmonic Response of Graphene in the Mid-Infrared. *Nano Lett.* **2013**, *13*, 1111–1117.
27. Xiao, S.; Chettiar, U. K.; Kildishev, A. V.; Drachev, V.; Khoo, I. C.; Shalaev, V. M. Tunable Magnetic Responseof Metamaterials. *Appl. Phys. Lett.* **2009**, *95*, 033115.
28. Khoo, I. C.; Diaz, A.; Stinger, M. V.; Huang, J.; Ma, Y. Liquid Crystal Tunable Optical Metamaterials. *IEEE J. Sel. Top. Quantum Electron.* **2010**, *16*, 410–417.
29. Kang, B.; Woo, J. H.; Choi, E.; Lee, H.-H.; Kim, E. S.; Kim, J.; Hwang, T.-J.; Park, Y.-S.; Kim, D. H.; Wu, J. W. Optical Switching of Near Infrared Light Transmission in Metamaterial-Liquid Crystal Cell Structure. *Opt. Express* **2010**, *18*, 16492–16498.
30. Zhang, F.; Zhang, W.; Sun, J.; Qiu, K.; Zhou, J.; Lippens, D. Electrically Controllable Fishnet Metamaterial Based on Nematic Liquid Crystal. *Opt. Express* **2011**, *19*, 1563–1568.
31. Minovich, A.; Farnell, J.; Neshev, D. N.; McKerracher, I.; Karouta, F.; Tian, J.; Powell, D. A.; Shadrivov, I. V.; Tan, H. H.; Jagadish, C.; *et al*. Liquid Crystal Based Nonlinear Fishnet Metamaterials. *Appl. Phys. Lett.* **2012**, *100*, 121113.
32. Decker, M.; Kremers, C.; Minovich, A.; Staude, I.; Miroshnichenko, A. E.; Chigrin, D.; Neshev, D. N.; Jagadish, C.; Kivshar, Y. S. Electro-Optical Switching by Liquid-Crystal Controlled Metasurfaces. *Opt. Express* **2013**, *21*, 8879–8885.
33. Liu, L.; Shadrivov, I. V.; Powell, D. A.; Raihan, R. M.; Hattori, H. T.; Decker, M.; Mironov, E.; Neshev, D. N. Temperature Control of Terahertz Metamaterials with Liquid Crystals. *IEEE Trans. Terahertz Sci. Technol.* **2013**, *3*, 827–831.
34. Buchnev, O.; Ou, J. Y.; Kaczmarek, M.; Zheludev, N. I.; Fedotov, V. A. Electro-Optical Control in a Plasmonic Metamaterial Hybridised with a Liquid-Crystal Cell. *Opt. Express* **2013**, *21*, 1633–1638.
35. Atorf, B.; Mühlenbernd, H.; Muldarisnur, M.; Zentgraf, T.; Kitzerow, H. Electro-Optic Tuning of Split Ring Resonators Embedded in a Liquid Crystal. *Opt. Lett.* **2014**, *39*, 1129–1132.
36. Li, J.; Wu, S.-T.; Brugioni, S.; Meucci, R.; Faetti, S. Infrared Refractive Indices of Liquid Crystals. *Appl. Phys.* **2005**, *97*, 073501.
37. Care, C. M.; Cleaver, D. J. Computer Simulation of Liquid Crystals. *Rep. Prog. Phys.* **2005**, *68*, 2665–2700.